nature nanotechnology

ARTICLES

PUBLISHED ONLINE: 21 NOVEMBER 2016 | DOI: 10.1038/NNANO.2016.239

# Tracking the dynamics of circulating tumour cell phenotypes using nanoparticle-mediated magnetic ranking

Mahla Poudineh[1], Peter M. Aldridge[2], Sharif Ahmed[3], Brenda J. Green[2], Leyla Kermanshah[2], Vivian Nguyen[3], Carmen Tu[3], Reza M. Mohamadi[3], Robert K. Nam[4], Aaron Hansen[5], Srikala S. Sridhar[5], Antonio Finelli[5], Neil E. Fleshner[5], Anthony M. Joshua[5], Edward H. Sargent[1]* and Shana O. Kelley[2,3,6]*

**Profiling the heterogeneous phenotypes of rare circulating tumour cells (CTCs) in whole blood is critical to unravelling the complex and dynamic properties of these potential clinical markers. This task is challenging because these cells are present at parts per billion levels among normal blood cells. Here we report a new nanoparticle-enabled method for CTC characterization, called magnetic ranking cytometry, which profiles CTCs on the basis of their surface expression phenotype. We achieve this using a microfluidic chip that successfully processes whole blood samples. The approach classifies CTCs with single-cell resolution in accordance with their expression of phenotypic surface markers, which is read out using magnetic nanoparticles. We deploy this new technique to reveal the dynamic phenotypes of CTCs in unprocessed blood from mice as a function of tumour growth and aggressiveness. We also test magnetic ranking cytometry using blood samples collected from cancer patients.**

The metastasis of cancerous tumours relies on the release of circulating cells that migrate to distant sites and form secondary tumours[1,2]. The factors that determine the invasiveness of these circulating tumour cells (CTCs) remain poorly defined, and it is not yet possible to distinguish CTCs that have high versus low metastatic potential. Studying CTCs that are directly collected from unprocessed blood samples is a challenge given their rarity (parts per billion) in the bloodstream[3,4]. Moreover, these cells are highly heterogeneous: multiple cell phenotypes can exist within a given tumour, and their properties evolve dynamically once they leave a tumour and enter the bloodstream[1].

Fluorescence-activated cell sorting (FACS) is a powerful present-day method to characterize and sort heterogeneous cell subpopulations. Unfortunately, FACS does not possess the sensitivity required to enable the routine characterization of CTCs at the levels at which they are present in the bloodstream, and is therefore not broadly applicable to the analysis of rare cells in clinical specimens. Microfluidics-based approaches have provided a new avenue to study CTCs[5–17]; however, existing techniques are generally limited to the capture and enumeration of CTCs and do not report on the phenotypic properties of CTCs.

New methods are urgently needed to characterize and sort CTCs according to their detailed phenotypic profiles so that the properties of invasive versus noninvasive cells can be identified. High levels of sensitivity and high resolution are required to generate profiles that will provide biological and clinical insights. We recently reported a method that allowed us to sort CTC subpopulations coarsely according to their phenotypic properties[18]. The resolution that was achieved, however, enabled discrimination among surface expression levels only when very large differences were at play. We hypothesized that much greater resolution would be required to accurately profile the phenotypes of CTCs to connect their molecular-level properties with invasiveness.

Here, we report a novel approach that exploits nanoparticle-mediated cell sorting, and relies on a unique chip architecture that achieves excellent control over an applied magnetic field along a channel. In this way, this new system accomplishes high-resolution phenotypic ranking of CTCs. We term the new approach, which is based on the longitudinal profile of magnetic field gradients, magnetic ranking cytometry (MagRC). MagRC generates a phenotypic profile of CTCs using information collected at the single-cell level. We show that it allows sorting of CTCs into one hundred different capture zones. We find that MagRC has a very high level of sensitivity and is able to profile CTCs accurately even when they are present at low levels (10 cells per ml) in unprocessed blood. The strategy allows the dynamic properties of CTCs to be tracked as a function of tumour growth and aggressiveness. Using blood samples both from xenografted mice and from human cancer patients, we show that the increased resolving power of MagRC provides distinct new information that is not accessible using existing methods.

## Overview of MagRC

The MagRC approach leverages immunomagnetic separation[19] for profiling CTCs as a function of their surface marker expression. A

[1]Department of Electrical and Computer Engineering, Faculty of Engineering, University of Toronto, Toronto, Ontario M5S 3G4, Canada. [2]Institute for Biomaterials and Biomedical Engineering, University of Toronto, Toronto, Ontario M5S 3M2, Canada. [3]Department of Pharmaceutical Science, Leslie Dan Faculty of Pharmacy, University of Toronto, Toronto, Ontario M5S 3M2, Canada. [4]Sunnybrook Health Sciences Centre, Sunnybrook Research Institute, University of Toronto, Toronto, Ontario M4N 3M5, Canada. [5]Princess Margaret Cancer Centre, University Health Network, University of Toronto, Toronto, Ontario M5G 2M9, Canada. [6]Department of Biochemistry, Faculty of Medicine, University of Toronto, Toronto, Ontario M5S 1A8, Canada.
*e-mail: shana.kelley@utoronto.ca; ted.sargent@utoronto.ca

whole blood sample is incubated with antibody-functionalized magnetic nanoparticles that bind specifically to a corresponding surface marker, and microengineered structures inside the device enable the rare cell profiling capability of MagRC. X-shaped structures within the microfluidic channel generate regions with slow flow and favourable capture dynamics[18], a requirement for the capture of cells that are tagged with magnetic nanoparticles; whereas highly discretized sorting of subpopulations is achieved via the introduction of differently sized nickel micromagnets[20]. The local magnetic force is engineered to vary systematically within the device via the footprint of the micromagnets (Fig. 1b,c). The micromagnets are positioned concentrically within the X-shaped microstructures, creating regions with low flow and high magnetic field gradients that are ideal for capturing CTCs with even low levels of magnetic loading (Fig. 1a). This device, coupled with immunostaining of captured cells, is intended to generate high-resolution profiles of cells captured from whole blood (Fig. 1d).

A quantitative physical model of the device (see Supplementary Figs 1–4) was developed to explore how cells exhibiting varied expression levels would generate different MagRC profiles that manifested their distinct phenotypes. A capture volume was defined as a region in which the magnitudes of the magnetic and drag forces are comparable. As a result, those cells that pass through a capture zone will be deflected and captured. For a cell covered with an abundance of bound magnetic nanoparticles, the capture zones generated by even the smallest micromagnets are sufficient to ensure complete capture in the earliest zones of the MagRC Chip (Fig. 1c, top). Cells with low surface marker expression are deflected only if they are close to edges of the micromagnets, where the magnetic force acting on the nanoparticles is highest (Fig. 1c, bottom). As each micromagnet is positioned concentrically with an X-structure, the regions in the MagRC chip that exhibit the highest magnetic forces and field gradients also correspond to the regions that exhibit the slowest flows. This has the benefit of creating localized regions with favourable capture dynamics (low drag and high magnetic forces), while also contributing to the high-resolution sorting capability of the chip.

For each cell in each zone, the probability of that cell encountering a capture region was calculated and reported as the capture parameter. Because the nickel micromagnets generate amplified magnetic fields near the bottom of the microfluidic channel, the capture parameter of a given cell within the chip depends strongly on its vertical position. Additionally, the extended length of the chip relative to its height leads to long residence times and the potential for cells to settle towards the bottom of the chip. The vertical dependence of the capture parameter for cells having different levels of magnetic loading is illustrated in Fig. 2a. Thousands of model cells were simulated, each having a randomly assigned initial height ranging from 5 to 45 μm at the inlet of the microfluidic chip. The overall modelling results presented in Fig. 2b show the predicted capture locations for three types of cells with high, medium and low levels of magnetic loading. (See Supplementary Information for a detailed explanation of the parametric model).

## Resolution, sensitivity and versatility of the MagRC approach

In a first suite of experiments, we used four cell lines with known levels of expression of the epithelial cell adhesion molecule (EpCAM) to challenge the capture and sorting capabilities of the MagRC chip. EpCAM is a surface marker that is commonly used to target CTCs. It is known that CTCs lose EpCAM when they undergo the epithelial to mesenchymal transition (EMT) during cancer progression[21,22], and therefore tracking this marker should allow EMT to be monitored. Four different target cell lines—MCF-7, SKBR3 (breast adenocarcinoma cells), PC-3 (human prostate cancer cell line) and MDA-MB-231 (a breast cancer cell line with mesenchymal characteristics that mimics triple negative breast cancer cells)—were incubated with 50 nm nanoparticles coated with anti-EpCAM in buffered solution. After capture, a nuclear stain was introduced into the chip to identify captured cells, and the capture efficiency was assessed by counting the captured cells using fluorescent microscopy. Experiments for each cell line were repeated three times. Figure 3a shows the fluorescent microscope images of an SKBR3 cell captured at the edge of a nickel micromagnet (where the magnetic field and field gradients are at a maximum).

The four different cell lines tested exhibited markedly different distributions within the device (Fig. 3b and Supplementary Fig. 5). High recoveries of the cells injected into the device are achieved (MCF-7 95 ± 5%, SKBR3 93 ± 4%, PC-3 91 ± 6%, MDA-MB-231 94 ± 5%; Fig. 3c), indicating that this approach has a high level of sensitivity. MCF-7 cells, which have the highest level of EpCAM expression, were found primarily in the earlier zones where the micromagnets are the smallest. However, PC-3 and MDA-MB-231 cells (which had the lowest level of EpCAM expression) were only captured after they encountered the large micromagnets closer to the outlet of the chip. The relative levels of EpCAM expression of the cell lines were confirmed via flow cytometry (FCM, inset to Fig. 3b). *T*-test analysis was used to assess the statistical significance of the MagRC profiles obtained from different cell lines (Supplementary Tables 1–3). The calculated *P* values (<0.0001) confirm the statistical significance of the uniqueness of the MagRC profiles and that the resolution of this technique is high. On the basis of these results we can conclude that the MagRC chip is able to sort cells according to the expression level of a targeted surface marker. Moreover, it efficiently captures cells that exhibit even low levels of a target surface marker, and can be applied widely to target surface markers for which a corresponding antibody is available.

This MagRC approach is amenable to the use of a wide range of surface antigens as the basis for profiling. We profiled the SKBR3 cell line using three different surface markers that are often expressed in epithelial cancer cells: human epidermal growth factor receptor 2 (HER2)/neu, EpCAM and N-cadherin (Fig. 3d). The inset in Fig. 3d shows the level of these three surface markers in SKBR3 cells measured by FCM. HER2 is known to be highly overexpressed in this cell line, and experiments with magnetic nanoparticles coated with anti-HER2 led to cell capture within the very earliest zones of the chip. In contrast, capture with anti-N-cadherin coated nanoparticles showed most cells being captured in the later zones of the chip. EpCAM levels are intermediate for these cells, a fact also reflected in the MagRC profiles.

The data presented indicate that MagRC produces profiles that are comparable to those reported by FCM. FCM is a powerful and robust approach useful in analysing protein expression and heterogeneity in living cells. It is limited in its sensitivity, however, and requires cell numbers of $10^4$ or higher for accurate results[23]. As shown here, MagRC reports on protein expression with a similar resolution, but using much smaller collections of cells. It is also noteworthy that the MagRC approach is a gentle analysis method that allows high recoveries of viable cells (Fig. 3e). 92% of captured cells can be recovered, and 98% of the recovered cells are viable (Supplementary Fig. 7).

We then proceeded to challenge the system using unprocessed whole blood samples, and found that MagRC retains its sensitivity and profiling capability. When whole blood samples (1 ml) containing between 10 and 40 cells were profiled using EpCAM as a target marker, reproducible profiles were obtained (Fig. 4). We compared the performance of the MagRC approach with the CTC gold standard FDA-cleared CellSearch assay (Fig. 4b). Spiked blood samples containing 100 SKBR3, PC-3 and MDA-MB-231 cells per millilitre were prepared and analysed using both the MagRC chip and CellSearch. High recoveries of the spiked samples injected into the MagRC chip

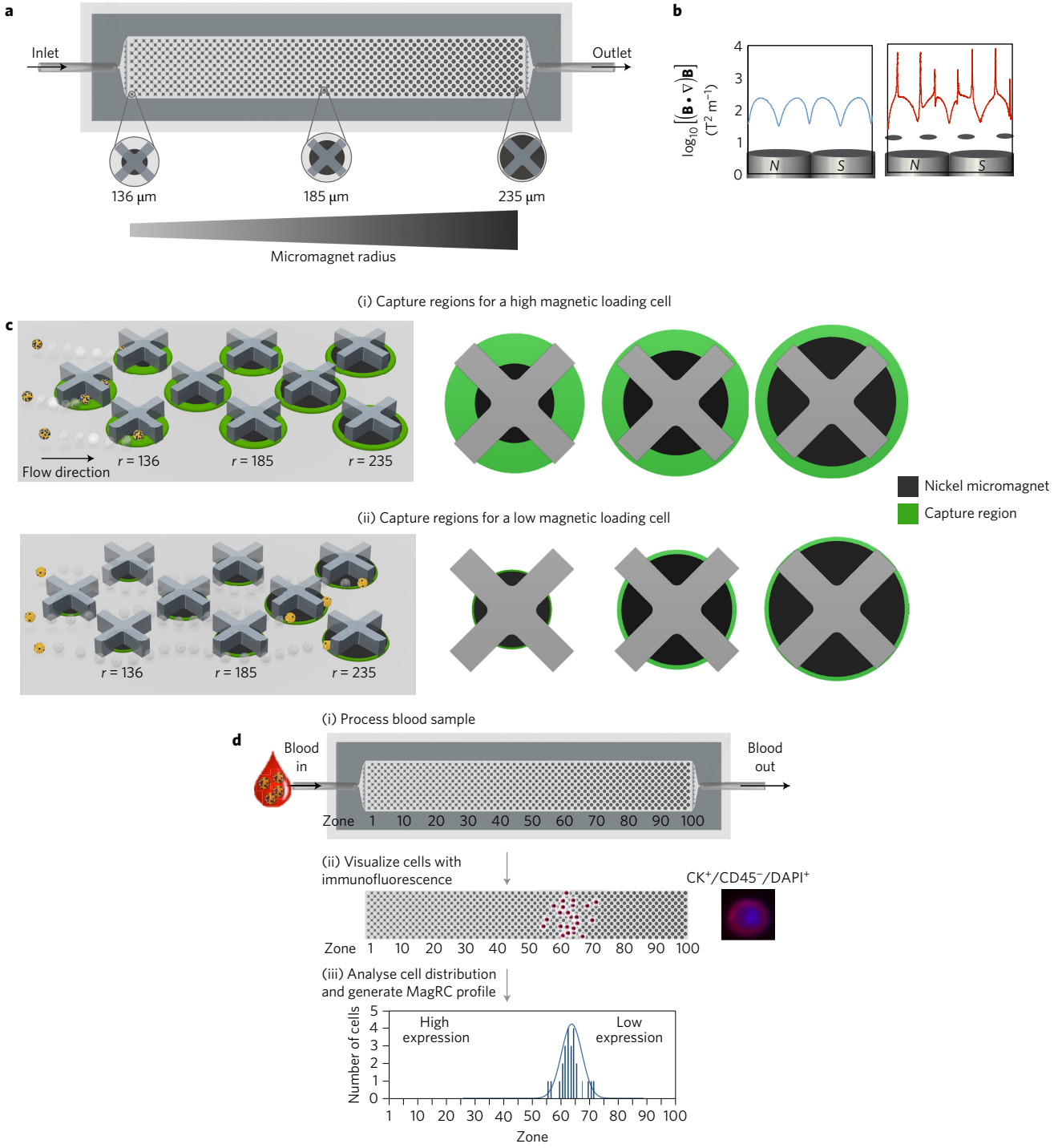


**Figure 1 | The MagRC approach to profiling rare cells. a**, The microfluidic chip used for MagRC contains 100 distinct zones with varied magnetic capture zones. An array of X-shaped structures generates regions of locally low velocity and circular nickel micromagnets patterned within the channel enhance the externally applied magnetic field. Increasing the size of the micromagnets along the channel increases their region of influence, where high magnetic field gradients lead to efficient CTC capture; these regions are termed capture zones. **b**, Comparison of the field gradient in the absence (left) and the presence (right) of Ni micromagnets. The micromagnets generate enhanced field gradients inside the microfluidic channel. The field gradient was measured at the channel height of 5 μm. B denotes magnetic field in the equation. **c**, Schematic representation of the capture zones in a condensed MagRC chip. The green annuli represent capture regions where cells with varied nanoparticle loadings are predicted to be captured efficiently. CTCs with high levels of surface marker expression experience larger effective capture regions as they flow through the chip. Cells with high levels of surface marker expression (and thus high magnetic loading) are captured in the earliest zones where the micromagnets are small (i, top), while for low expression cells, the larger micromagnets encountered later in the chip are required to generate a sufficiently large capture region (ii, bottom). *r* denotes the micromagnet radius. **d**, Overview of the MagRC approach. (i) Whole, unprocessed blood is introduced into the microfluidic chip. Once the sample has been processed, the chip is washed with buffer. (ii) Immunostaining is then used to identify CTCs and their distribution within the chip. (iii) The number of cells in each zone is then tabulated and used to generate a profile that reflects the levels of protein expression for the cells as a collective.

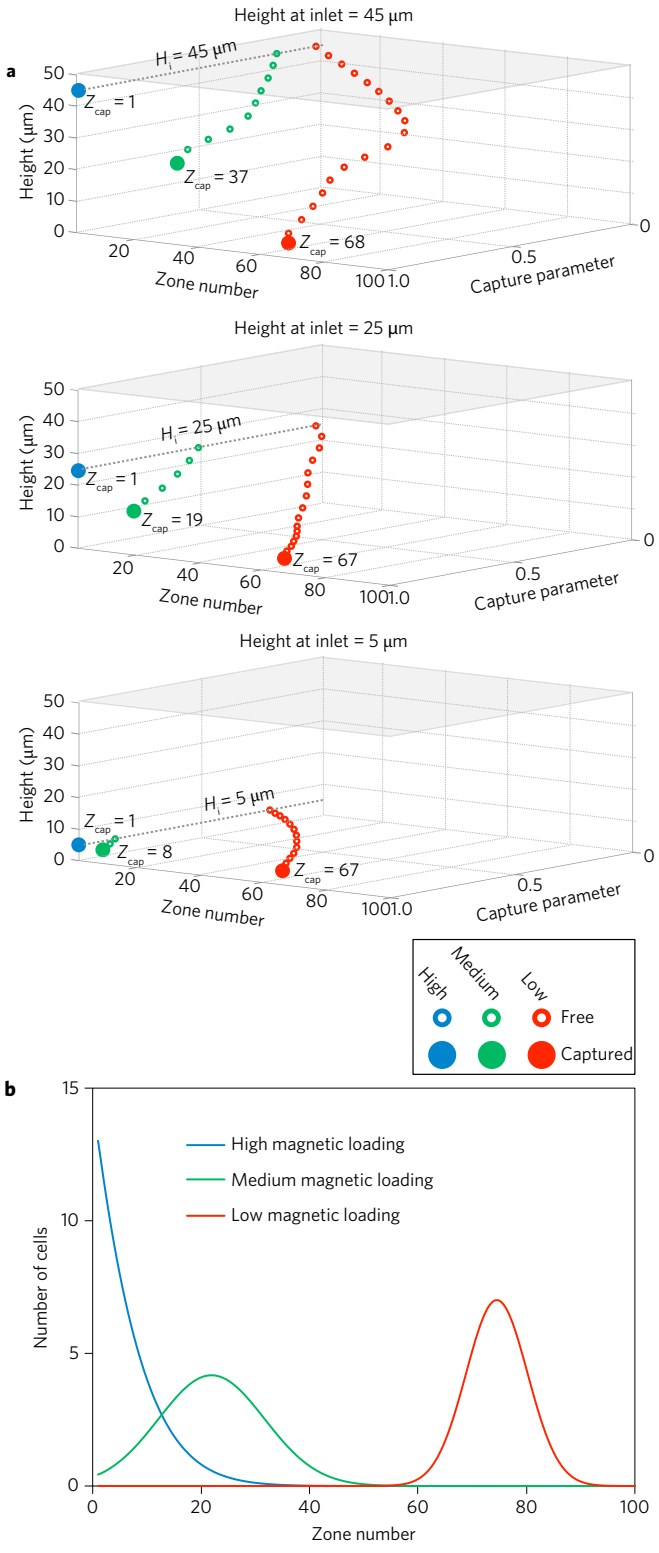


**Figure 2 | Modelling of cell capture in the MagRC device. a**, Normalized capture parameter as a function of height and capture zone ($Z_{cap}$) in the chip, for three different inlet heights ($H_i$). **b**, A parametric model predicts where cells with high, medium and low magnetic loads will be captured in the MagRC chip. See Supplementary Information and Supplementary Figs 1–3 for an explanation of the model and modelling data.

were achieved (SKBR3 97 ± 3%, PC-3 90 ± 2%, MDA-MB-231 90 ± 3%). The efficient capture of MDA-MB-231 and PC-3 cells, which have a low level of EpCAM, indicates that low-EpCAM cells presented in whole blood samples would still be visualized with this technique. However, in contrast, the CellSearch system exhibits significantly suppressed capture efficiencies with low-EpCAM cells.

To further validate the phenotypic profiling performance of the MagRC approach in whole blood, we performed head-to-head studies of blood samples containing 100 cancer cells where both MagRC and FCM were used for profiling. MagRC profiled cells in the presence of normal blood cells (Fig. 4c–e), while FCM was unable to report a specific signal (Fig. 4e). Even in the presence of 10,000 cells spiked into blood, a specific signal was not obtained using FCM. Only after the blood was treated to lyse red blood cells could spiked cancer cells be visualized; unfortunately, this processing step eliminates over 50% of the cancer cells (Supplementary Fig. 8), and therefore creates a considerable potential for false negatives. In contrast to FCM, the MagRC approach provides accurate profiling even with very low levels of cancer cells in unprocessed blood. This is a requirement for the evaluation of CTCs. It is noteworthy that the exact shape of the profile returned with MagRC is affected by the presence of blood cells (Fig. 4e); however, as it is affected in a consistent and predictable fashion by the increased drag acting on the tumour cells that arises from interactions with the blood cells, it gives reproducible data for a given type of sample (for example, whole blood).

The purity of the cancer cells recovered during MagRC profiling was assessed by counting the numbers of white blood cells (WBCs) that are non-specifically captured within our devices. The MagRC chip depletes up to 99.98% of the WBCs, with approximately 2,000 WBCs found in the chip after processing 1 ml of blood. Although much of this contamination is derived from the non-specific binding of WBCs to the device, we wondered whether the non-specific binding of magnetic beads could also contribute to the capture of these cells. We used FCM to compare the specific binding of particles to MDA-MB-231 cells and the non-specific binding to WBCs (Supplementary Fig. 4). The data from this experiment indicated that the level of non-specific binding of the magnetic nanoparticles to WBCs is approximately ten times lower than that occurring on low-EpCAM cells, indicating that WBCs would not be captured within our device via this mechanism. The level of WBC contamination found in the MagRC chip is comparable to other microfluidic capture approaches, including the micropost CTC chip with ~640 WBCs isolated per 1 ml of blood[6], the microvortex-generating herringbone-chip with 4,500 WBCs isolated per millilitre[9] and the tunable nanostructured coating approach with 1,200 WBCs isolated per millilitre[14]. For our approach, along with the others described where a positive selection approach is used, the ability to identify cancer cells specifically using immunofluorescence ensures that these non-specifically bound cells do not contribute to the results obtained.

## Monitoring dynamic CTC phenotypes in an animal model

To evaluate the utility of MagRC for the analysis of CTCs and their dynamic properties, we first analysed blood from mice bearing xenografted tumours as a function of tumour growth. To generate the model, we implanted MCF-7/Luc human breast cancer cells into the mammary fat pad of immunodeficient mice. One group of mice received an estrogen pellet before tumour implantation (E+), as estrogen stimulates MCF-7 tumour growth. Mice in the other set were not treated with estrogen before tumour implantation (E–). After tumour cell injection, we collected blood from each mouse every 10 days and analysed the samples using MagRC. Immunostaining that was specific for the implanted human cancer cells was used to establish the MagRC profile (Fig. 5a), and tumour growth was visualized by imaging the bioluminescence generated by the luciferin-tagged MCF-7 cells (Fig. 5b).

As tumour growth progressed in the xenografted animals, a marked change was visualized in the CTCs detected. In both the E+ and

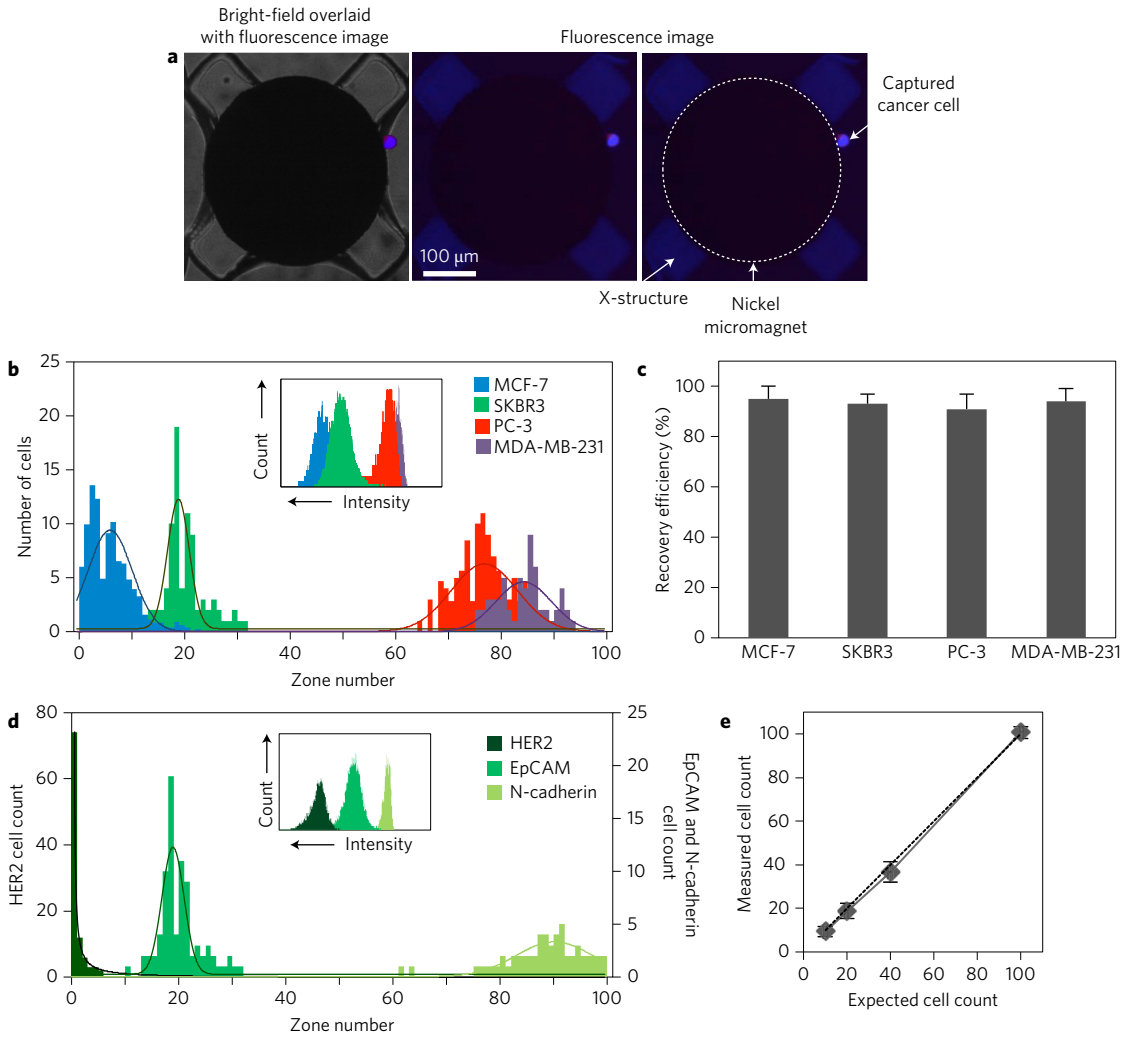


**Figure 3 | Profiling protein surface expression using MagRC. a**, Bright-field (left) and fluorescent (right) microscope images of a captured immunostained SKBR3 cell. **b**, Distribution of MCF-7, SKBR3, PC-3 and MDA-MB-231 cells in the MagRC chip; EpCAM was used as the profiling marker. One hundred cells suspended in 100 µl of buffer were used in these trials. Profiling experiments for each cell line were repeated five times. Three replicates for capturing each cell line are shown in Supplementary Information. Inset, EpCAM expression measured by FCM for the three cell lines. **c**, Capture efficiency for cells that have different levels of EpCAM expression. The high recovery of low-EpCAM cells (MDA-MB-231 and PC-3) proves the suitability of the MagRC approach for monitoring cells with lowered epithelial markers. **d**, SKBR3 cells were profiled for different cancer biomarkers using three capture antibodies: EpCAM, HER2 and N-cadherin. One hundred cells suspended in 100 µl of buffer were used in these trials, and experiments were replicated three times. Inset, Expression of the same three markers on SKBR3 cells measured by FCM. **e**, The sensitivity of the MagRC approach was tested by spiking different numbers of SKBR3 cells in the buffer solution and counting them using immunofluorescence after capture in a MagRC chip. A low number of cells ($n = 10$) spiked into a volume of 100 µl can be visualized. Error bars show standard deviations, $n = 3$. It is noteworthy that overlap can occur for the profiles collected from different cell lines, reflecting that surface expression levels for some cell subpopulations in different cell lines may be similar. As shown in the inset of **b**, FCM also generates overlapping profiles.

E− animal groups, CTC levels rose as the study progressed. In the E+ group, as expected, the CTCs levels increased to a much higher level than in the estrogen-negative group. Notably, in addition to increasing in number, the more aggressive cancer model also exhibited a marked phenotypic shift: the CTCs profiled in these mice were localized in later zones within the MagRC microfluidic chip compared with early CTCs and cultured MCF-7 cells (Fig. 3b and Supplementary Fig. 9). The profiles indicate that the phenotypes of the CTCs were changing and EpCAM levels were decreasing (Fig. 5c, Supplementary Figs 10 and 11). The profiles of the CTCs from the E− mice remained static (Fig. 5d, Supplementary Figs 10 and 11).

To compare the invasiveness of the tumours in the two groups, we extracted mouse lungs and sent them for histopathology at the end of the study; these sections were then scanned for micrometastases. Micrometastases were found in lungs of the E+ group (Fig. 5e,f); and there were no micrometastases in the E− group. The presence of the metastases along with the altered CTC profile observed by MagRC is consistent with the hypothesis that the CTCs produced by the E+ tumours possess a more invasive profile.

## Profiling phenotypes of CTCs in clinical samples

To evaluate the performance of MagRC when tested with clinical samples, we conducted a study of samples collected from patients exhibiting metastatic castration-resistant prostate cancer (mCRPC, $n = 10$) and localized prostate cancer, ($n = 14$, Fig. 5g–i and Supplementary Tables 5 and 6). Immunostaining was used to distinguish between CTCs and WBCs (Fig. 5g). We also analysed the blood collected from nine healthy donors (Supplementary Table 4).

The profiles collected from the different patients exhibited an interesting series of trends (Fig. 5). Overall, the MagRC profiles for the

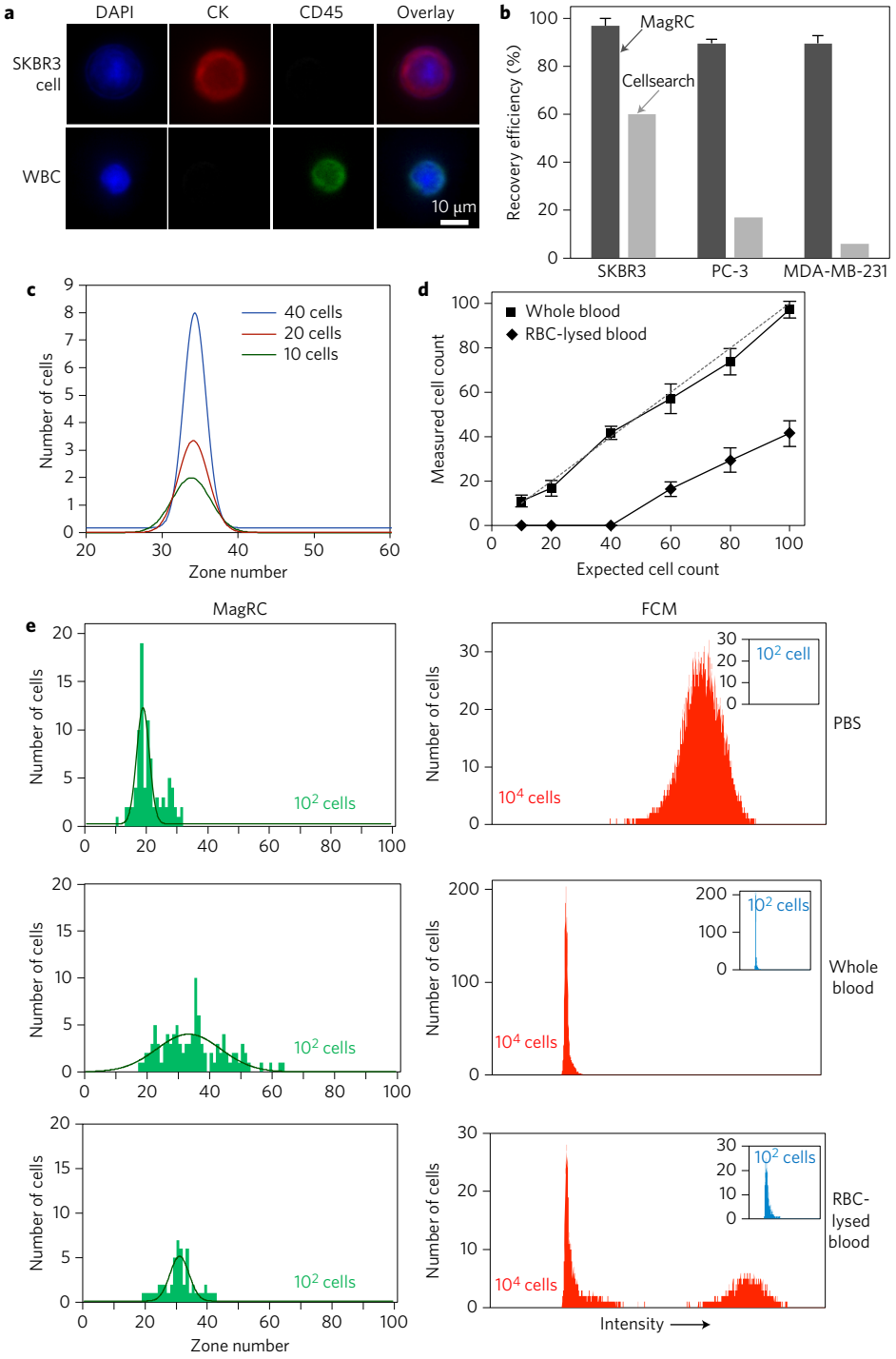


**Figure 4 | MagRC applied to rare cells in whole blood. a**, Specific immunostaining of cancer cells. After capture, cancer cells are stained for DAPI, CK and CD45. SKBR3 cells were identified as $DAPI^+/CK^+/CD45^-$ and white blood cells were identified as $DAPI^+/CK^-/CD45^+$. **b**, Head-to-head comparison of the MagRC chip with CellSearch. One hundred cells of SKBR3, PC-3 and MDA-MB-231 cells were spiked into whole blood. MagRC and CellSearch were used to count cells. CellSearch was inefficient to recover low EpCAM cells while MagRC retains cells with efficiency more than 90%. **c**, Different numbers of SKBR3 cells were spiked in 1 ml of whole blood and the MagRC chip was used to profile the spiked samples for surface expression of EpCAM. Experiments were repeated three times. **d**, MagRC was used to count rare cells in unprocessed whole blood samples and red blood cell (RBC)-lysed samples. A significant proportion of cells are lost when this sample processing step is used. In unprocessed blood, MagRC shows high levels of sensitivity and linearity. See Supplementary Fig. 8 for raw data. Cells were spiked into 1 ml of human blood for all trials shown. Error bars show standard deviations, $n = 3$. The dashed line shows the ideal 100% capture efficiency and the solid lines show the counts extracted from the MagRC chip. **e**, The MagRC chip (left) and FCM (right) were used to monitor cells in PBS (top), whole blood (middle) and RBC-lysed blood (bottom). The MagRC chip was able to accurately profile cells in all three solutions. However, the background signal for the whole blood samples overwhelmed the signals collected via FCM; only cells in PBS and RBC-lysed blood samples were accurately measured using the technique. Owing to the inability of FCM to accurately count low (~100) numbers of spiked cells (inset), samples with a higher level of SKBR3 cells ($10^4$) were measured and counted using FCM. Profiling with both FCM and MagRC was repeated three times. The curves in the MagRC profiles present the normal distribution fit to the count data.

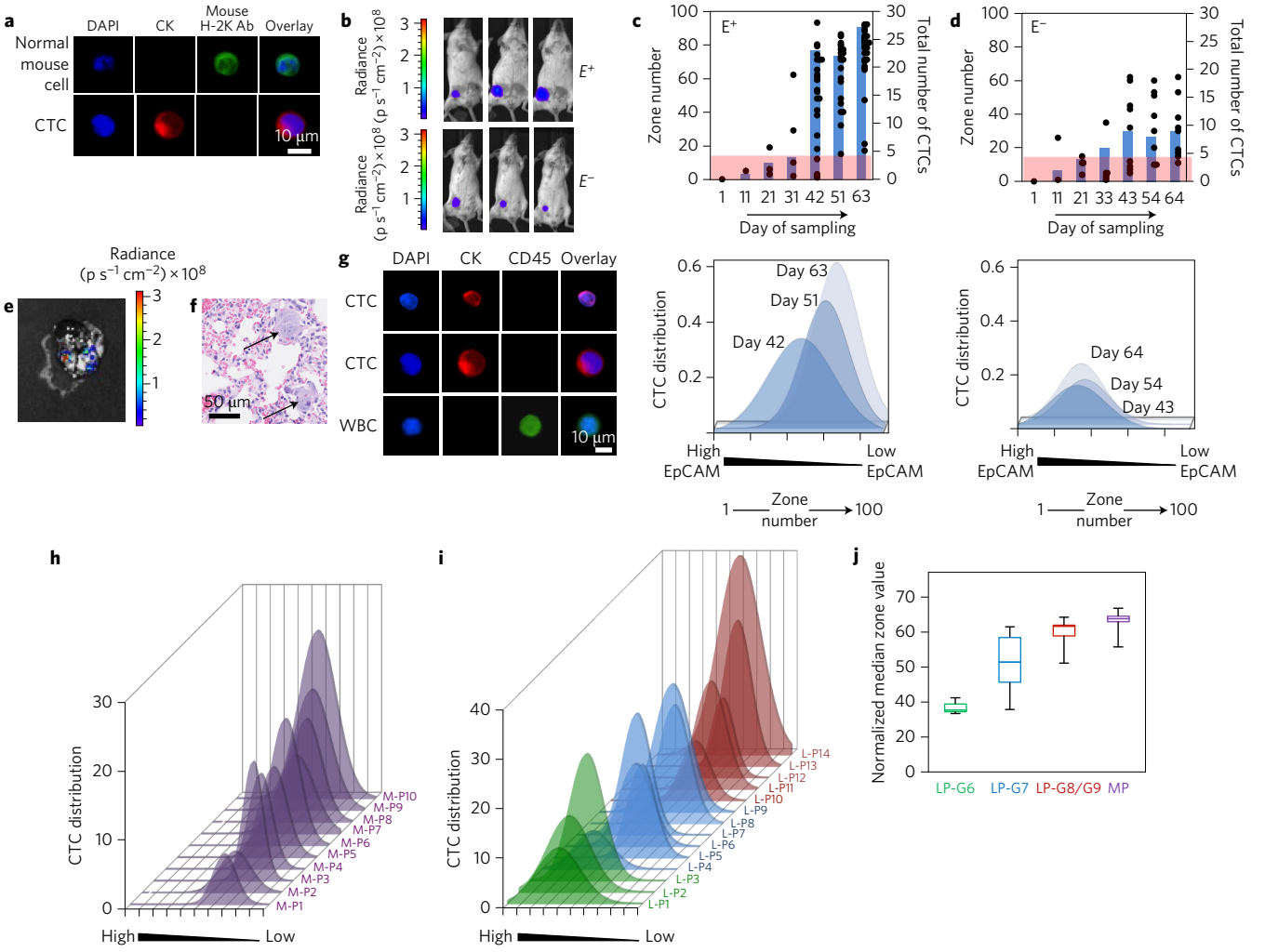


**Figure 5 | MagRC enables profiling of CTCs in cancer xenograft models and patient samples. a**, Representative images of a captured CTC and a normal mouse cell. Nuclei are stained with DAPI (blue), CTCs are stained for CK (red) and mouse cells for mouse H-2k (green). **b**, Bioluminescence images of mice implanted with MCF-7 tumours in the E+ and E– groups during the course of tumour progression. p in the unit denotes photons. **c**,**d**, CTC distribution profiles of mice in the E+ and E– groups. Bar graphs show the total number of CTCs found each day. Each black circle denotes one CTC. The red zone represents the distribution area for cultured MCF-7 cells (see Supplementary Fig. 9). Scaled normal distribution profiles of CTCs extracted at each time point are shown below, centred at the median CTC zonal position. CTC profiles in the E+ model show a shift towards less epithelial phenotypes at the later stages of the disease (**c**), however, this shift is not observed in the E– model (**d**). See Supplementary Figs 10 and 11 for additional data collected with animals. As our sample size (the number of mice) is less than five, we have not used any statistical analysis and individual data points were plotted. **e**, Bioluminescence image of the whole lung of a mouse in the E+ group. Visible luminescence indicates the presence of metastases in the lung. **f**, Histopathology image of a lung section of a mouse from the E+ group confirming the presence of micrometastases. The arrows point to the micrometastases. **g**, Representative images of CTCs captured from prostate cancer patient samples versus a white blood cell. Nuclei are stained with DAPI (blue), CTCs are stained for CK (red) and WBCs for CD45 (green). **h**, EpCAM profiles for CTCs captured from samples from patients with mCRPC ($n = 10$). See Supplementary Table 6 for patient data. **i**, EpCAM profiles for CTCs captured from samples from patients with localized prostate cancer ($n = 14$). See Supplementary Table 5 for patient data. Patients with tumours with a Gleason score of 6 are coloured green (P1–P3), with a Gleason score of 7 are blue (P4–P9) and with Gleason scores of 8 and 9 are red (P10–P14). See Supplementary Fig. 12 for the mean capture zone values and Supplementary Table 7 for statistical analysis of these values. **j**, Box plot indicating the median values that correspond to capture profiles for localized prostate cancer patients with Gleason score 6 tumours (LP-G6), Gleason score 7 tumours (LP-G7), Gleason score 8 or 9 tumours (LP-G8/G9) or mCRPC patients (MP). Error bars in the box plot show the range of CTC counts in each group.

mCRPC patients were similar to one another (Fig. 5h). The CTCs from these patients appeared in the later zones of the device, consistent with the idea that these were low-EpCAM CTCs in later stages of the EMT. In the case of localized prostate cancer patients, there was an appreciably greater diversity in the MagRC profiles (Fig. 5i) when CTCs were detected. We analysed the profiles according to the Gleason score of the tumours biopsied in these patients. Three, six, and five patients with tumours with Gleason score of 6 (P1–P3), a Gleason score of 7 (P4–P9) and Gleason scores of 8 and 9 (P10–P14) were analysed, respectively. We measured the zone distribution profile for these patients and found that G6 patient CTCs were captured in earlier zones (median zone = 40) relative to the CTCs captured from samples from patients with G8/G9 tumours (median zone = 64) (Supplementary Fig. 12). The box plot presented in Fig. 5j also demonstrates the CTC profile distribution in patients with different types of prostate cancer tumours. These results suggest that the patients with G7 tumours exhibited variable profiles compared with the other two groups. We performed statistical analysis on the localized prostate cancer patient CTC zone distributions and found that G8–G9 CTCs were statistically separated from G6 CTCs (Supplementary Table 7, $P < 0.05$, paired $t$-test). The mean values of the G7 tumour profiles did not exhibit statistical significance from the G6 or G8/G9

patients, indicating significant phenotypic heterogeneity for the G7 patients. This is an interesting finding because G7 patients have variable prognoses; while 50% of patients with G7 tumours do experience cancer recurrence, 50% do not[24]. A much larger study will be necessary to determine whether there is a correlation between the CTC phenotypic profiles we are measuring and recurrence, but the analysis of CTC phenotypes for these patients may help to elucidate the differences between tumours with similar staging data.

## Conclusions

The high level of sensitivity we report for phenotypic profiling of CTCs using MagRC, and the device's efficacy in the analysis of whole blood, render this a technique of interest in the analysis of rare CTCs. CTCs collected from mice with xenografted tumours were monitored as a function of tumour growth, and dynamic phenotypic profiles were observed for cells collected from animals with aggressive tumours. In samples collected from prostate cancer patients, MagRC enabled the sensitive profiling of CTCs and monitoring of changes in the CTC levels and phenotypes. A comparison of the CTCs profiled in samples collected from patients with localized versus metastatic prostate cancer revealed that there was much greater diversity in the phenotypes of CTCs for the former group.

The MagRC approach could be adapted to a variety of applications. Because an external magnetic field modulates CTC capture, cells can readily be recovered once the field is removed, thereby facilitating further offline analysis and culture. This technique is highly versatile as it can employ available antibodies to generate a MagRC profile, which makes it applicable to CTC analysis relevant to a variety of disease states. The new technique can be implemented using standard syringe pumps and fluorescence imaging interfaced with a microfluidic chip that is straightforward to fabricate and without the requirement for custom instrumentation. Further effort at system integration will permit deployment of this technology in clinical research and clinical cancer management.

MagRC is the first technique to provide accurate in-line profiles of low levels of CTCs in unprocessed blood samples. Although techniques developed previously have leveraged surface-bound magnetic particles for CTC enumeration[13,25], none have achieved the level of sensitivity and resolution that MagRC exhibits. Furthermore, none have provided the ability to report a protein expression profile for CTCs. MagRC provides information that is consistent with that provided by the existing gold standard method, FCM, and also allows vastly lower cell numbers to be queried. Further, the acquisition of sensitive information using MagRC is not degraded by the presence of an abundance of blood cells, thereby overcoming a significant limitation of FCM.

## Methods

Methods and any associated references are available in the online version of the paper.

Received 19 March 2016; accepted 3 October 2016; published online 21 November 2016

## References


1. Chaffer, C. L. & Weinberg, R. A. A perspective on cancer cell metastasis. *Science* **331,** 1559–1564 (2011).
2. Plaks, V., Koopman, C. D. & Werb, Z. Circulating tumor cells. *Science* **341,** 1186–1188 (2013).
3. Alix-Panabières, C. & Pantel, K. Challenges in circulating tumour cell research. *Nat. Rev. Cancer* **14,** 623–631 (2014).
4. Lang, J. M., Casavant, B. P. & Beebe, D. J. Circulating tumor cells: getting more from less. *Sci. Transl. Med.* **4,** 141ps13 (2012).
5. Green, B. J. *et al.* Beyond the capture of circulating tumor cells: next-generation devices and materials. *Angew. Chem. Int. Ed.* **55,** 1252–1265 (2016).
6. Hu, X. *et al.* Marker-specific sorting of rare cells using dielectrophoresis. *Proc. Natl Acad. Sci. USA* **102,** 15757–15761 (2005).
7. Nagrath, S. *et al.* Isolation of rare circulating tumour cells in cancer patients by microchip technology. *Nature* **450,** 1235–1239 (2007).
8. Adams, A. *et al.* Highly efficient circulating tumor cell isolation from whole blood and label-free enumeration using polymer-based microfluidics with an integrated conductivity sensor. *J. Am. Chem. Soc.* **130,** 8633–8641 (2008).
9. Talasaz, A. H. *et al.* Isolating highly enriched populations of circulating epithelial cells and other rare cells from blood using a magnetic sweeper device. *Proc. Natl Acad. Sci. USA* **106,** 3970–3975 (2009).
10. Stott, S. L. *et al.* Isolation of circulating tumor cells using a microvortex-generating herringbone-chip. *Proc. Natl Acad. Sci. USA* **107,** 18392–18397 (2010).
11. Wang, S. *et al.* Highly efficient capture of circulating tumor cells by using nanostructured silicon substrates with integrated chaotic micromixers. *Angew. Chem. Int. Ed.* **50,** 3084–3088 (2011).
12. Schiro, P. G. *et al.* Sensitive and high-throughput isolation of rare cells from peripheral blood with ensemble-decision aliquot ranking. *Angew. Chem. Int. Ed.* **51,** 4618–4622 (2012).
13. Zhao, W. *et al.* Bioinspired multivalent DNA network for capture and release of cells. *Proc. Natl Acad. Sci. USA* **109,** 19626–19631 (2012).
14. Ozkumur, E. *et al.* Inertial focusing for tumor antigen-dependent and -independent sorting of rare circulating tumor cells. *Sci. Transl. Med.* **5,** 179ra47 (2013).
15. Reátegui, E. *et al.* Tunable nanostructured coating for the capture and selective release of viable circulating tumor cells. *Adv. Mater.* **27,** 1593–1599 (2015).
16. Mittal, S., Wong, I. Y., Yanik, A. A., Deen, W. M. & Toner, M. Discontinuous nanoporous membranes reduce non-specific fouling for immunoaffinity cell capture. *Small* **9,** 4207–4214 (2013).
17. Schneider, J. *et al.* A novel 3D integrated platform for the high-resolution study of cell migration plasticity. *Macromol. Biosci.* **13,** 973–983 (2013).
18. Mohamadi, R. M. *et al.* Nanoparticle-mediated binning and profiling of heterogeneous circulating tumor cell subpopulations. *Angew. Chem. Int. Ed.* **54,** 139–143 (2015).
19. Ferguson, B. S. *et al.* Genetic analysis of H1N1 influenza virus from throat swab samples in a microfluidic system for point-of-care diagnostics. *J. Am. Chem. Soc.* **133,** 9129–9135 (2011).
20. Chen, P., Huang, Y.-Y., Hoshino, K. & Zhang, J. X. J. Microscale magnetic field modulation for enhanced capture and distribution of rare circulating tumor cells. *Sci. Rep.* **5,** 8745 (2015).
21. Santisteban, M. *et al.* Immune-induced epithelial to mesenchymal transition in vivo generates breast cancer stem cells. *Cancer Res.* **69,** 2887–2895 (2009).
22. Yu, M. *et al.* Circulating breast tumor cells exhibit dynamic changes in epithelial and mesenchymal composition. *Science* **339,** 580–584 (2013).
23. Jaye, D. L., Bray, R. A., Gebel, H. M., Harris, W. A. C. & Waller, E. K. Translational applications of flow cytometry in clinical practice. *J. Immunol.* **188,** 4715–4719 (2012).
24. Chan, T. Y., Partin, A. W., Walsh, P. C. & Epstein, J. I. Prognostic significance of Gleason score 3+4 versus Gleason score 4+3 tumor at radical prostatectomy. *Urology* **56,** 823–827 (2000).
25. Issadore, D. *et al.* Ultrasensitive clinical enumeration of rare cells *ex vivo* using a micro-hall detector. *Sci. Transl. Med.* **4,** 141ra192 (2012).


## Acknowledgements

The authors acknowledge generous support from the Canadian Institutes of Health Research (Emerging Team grant, POP grant), the Ontario Research Fund (ORF Research Excellence grant), the Canadian Cancer Society Research Institute (Innovation grant) and the Connaught Foundation. We also acknowledge all of the patients and healthy donors who donated specimens to our studies.

## Author contributions

M.P., P.M.A., S.A., B.J.G., L.K., V.N., C.T., R.M.M., S.O.K. and E.H.S. conceived and designed the experiments. M.P., P.M.A., S.A. B.J.G., L.K., V.N., C.T. and R.M.M. performed the experiments and analysed the data. R.K.N., A.H., S.S.S., A.F., N.E.F. and A.M.J. contributed clinical expertise and clinical specimens. All authors discussed the results and contributed to the preparation and editing of the manuscript.

## Additional information

Supplementary information is available in the online version of the paper. Reprints and permissions information is available online at www.nature.com/reprints. Correspondence and requests for materials should be addressed to E.H.S. and S.O.K.

## Competing financial interests

The authors declare no competing financial interests.

## Methods

**MagRC microfluidic chip fabrication.** Glass slides coated with a 1.5 μm Ni layer (EMF-Corp) were used to fabricate the MagRC chip. A topcoat of positive photoresist (AZ1600) was used. Contact lithography was used to pattern the micromagnets. After exposure for 10 s, the photoresist was developed. This was followed by Ni wet etching and removal of the top resist. To pattern the X-structures, a layer of negative photoresist, SU-8 3050 (Microchem) was spin-coated on top of the nickel coated glass substrates followed by 30 min of soft-baking. The final thickness of SU-8, and thus the height of channel, was 50 μm. After exposing for 20 s, the SU-8 layer was developed using SU-8 developer. The channel was finally topped with a layer of polydimethylsiloxane (PDMS). Holes were punched for the inlet and outlet in the PDMS layer.

**Cancer cell lines.** MCF-7/Luc human breast cancer cells were purchased from Cell Biolabs Inc. and grown in DMEM (high glucose) supplemented with 10% FBS, 0.1 mM MEM non-essential amino acids (NEAA) and 2 mM L-glutamine. The SKBR3 cell line was obtained from American Type Culture Collection (ATCC). SKBR3 cells were cultured in McCoy's 5a medium modified (ATCC). The medium was supplemented with 10% fetal bovine serum (FBS). Human prostate cancer cells PC-3 (a gift from A. Allan, London Health Sciences Centre) were cultured in F12K media (ATCC) supplemented with 10% FBS. All cell lines were authenticated using gene expression profiling and checked for microbial contaminations.

**Assessing the level of magnetic beads adsorption to WBC.** Fresh blood was collected from healthy donors and RBCs were lysed using 0.5 M EDTA, pH 8. MDA-MB-231 and SKBR3 cells also were prepared with the concentration of $10^5$ cells per millilitre in PBS plus 1% BSA. Then 10 μl of anti-EpCAM nano-beads (MACS) and 20 μl of FcR blocking reagent (MACS) were added to the samples (MDA-MB-231 cells, SKBR3 cells and RBC-lysed blood) and incubated for 30 min. After a washing step, the samples were incubated for another 30 min with 1.5 μl of Anti-mouse H-2Kd- Alexa Fluor 488 that served as the secondary antibody. This was followed by injection of the samples into the flow cytometer. Counts versus fluorescence intensity measurements were made in the green channel of the flow cytometer.

**Spiking of tumour cells in whole blood.** Fresh blood was collected from healthy volunteers and immediately used for experiments. Different numbers of SKBR3 cells were spiked into whole blood. After this step, some samples underwent an additional RBC lysis step; 1 ml of RBC lysis buffer was used, and this was followed by two washing steps with PBS. Lastly, both whole and RBC-lysed blood samples were run through the MagRC chip and analysed via FCM.

**Orthotropic tumour xenograft model and CT imaging.** All animal experiments were carried out in accordance with the protocol approved by the University of Toronto Animal Care Committee. Six- to eight-week-old female SCID-beige mice were purchased from Charles River and maintained at the University of Toronto animal facility. Two days before tumour implantation, the subset of mice received a subcutaneous pellet of 60–d sustained release 17-β-estradiol (0.72 mg per pellet; Innovative Research of America). Tumour xenografts were generated by injecting $5 \times 10^6$ cells suspended in 50 μl of Matrigel (BD Biosciences) orthotopically into the fourth left inguinal mammary fat pad. Mice were anaesthetized by isoflurane before injection. Tumour growth was measured both by caliper and by imaging using a Xenogen IVIS Spectrum imaging system (Caliper Life Sciences). If tumour growth was not observed in a mouse, it was excluded from the rest of study. Before imaging, mice were injected intraperitoneally with 100 μl of PBS containing D-Luciferin substrate (PerkinElmer). At the end of the experiment, animals were euthanized and selected tissues were analysed by *ex vivo* imaging for micro-metastasis detection. For intermediate CTC capture from tumour bearing mice, 50–100 μl of blood was collected from the saphenous vein and for the terminal studies 0.5–1 ml blood was collected from each mouse by cardiac puncture. All blood samples were collected in K2EDTA tubes (Microvette). During the animal study, randomization was not applied.

**Profiling of mouse CTCs and immunostaining.** Collected mouse blood was diluted with PBS-EDTA (100 μl of PBS-EDTA was added to 50 μl of blood). This was followed by adding 10 μl of anti-EpCAM nano-beads to 150 μl of diluted blood. After 30 min of incubation with the magnetic beads, blood was pumped through the MagRC Chip at a flow rate of 500 μl $h^{-1}$. Next, 200 μl PBS-EDTA was introduced to flush away any non-magnetically captured non-target cells. Captured cells were then fixed with 4% paraformaldehyde, and then permeabilized with 0.2% Triton X-100 (Sigma-Aldrich) in PBS. Anti-CK-APC (GeneTex) antibody was used to stain CTCs, and mouse cells were marked by anti-mouse-H-2K-FITC antibody to distinguish with CTCs. All antibodies were prepared in 100 μl of PBS and pumped through the chip at a flow rate of 50 μl $h^{-1}$ for 2 h. After immunostaining, chips were washed using 0.1% Tween 20 in PBS. Cell nuclei were stained with 100 μl DAPI ProLong Gold reagent (Invitrogen, CA) at 500 μl $h^{-1}$. After the staining was complete all of the chips were washed with PBS and stored at 4 °C before scanning.

**Image scanning and analysis.** After immunostaining, chips were scanned using a Nikon microscope under a ×10 objective, and images were acquired with NIS-Elements AR software. Bright-field, red (APC channel), green (FITC channel) and blue fluorescence images were recorded. The captured images were then analysed manually and target and non-target cells were counted.

**Histopathology of mouse tumours.** After terminal blood collection, animals were euthanized and lungs, liver, lymph nodes were extracted and fixed in 10% buffered formalin. Fixed tissues were then embedded in paraffin for histological examination with hematoxylin and eosin (H&E) staining. The pathologist was blinded to the different groups of animals during the study.

**Patient sample collection.** Patients with mCRPC were recruited from the Princess Margaret Hospital according to the University's Research Ethics Board approved protocol, and localized prostate cancer patients were recruited from Sunnybrook Hospital under an approved protocol. All patients were enrolled following informed consent. 20 ml peripheral blood samples from castration-resistant prostate cancer patients ($n = 10$) were used to validate CTC detection with MagRC versus CellSearch. Blood samples were collected in two CellSearch tubes that contained the anticoagulant EDTA (Johnson and Johnson). One tube of blood was shipped to the London Regional Cancer Program at the London Health Sciences Centre for CellSearch analysis, and the other tube of blood was processed using MagRC. 10 ml peripheral blood samples from localized prostate cancer patients ($n = 14$) were also analysed using MagRC. All samples were analysed within a 96 h window, typically within 24–48 h after blood collection. Blood from ten healthy donors was also analysed for comparison.

**CTC capture from patient samples.** 10 μl of anti-EpCAM Nano-Beads (MACS) and 20 μl of FcR Blocking Reagent (MACS) were added to 1 ml of blood and incubated for 30 min on a sample mixer. The blood was then introduced into a microfluidic device based on a simplified design[24] at a flow rate of 600 μl $h^{-1}$ using a syringe pump. Next, 400 μl of PBS-EDTA was added at a flow rate of 600 μl $h^{-1}$ to remove non-target cells. After this step, the chips were immunostained as detailed below.

**Immunostaining of patient CTCs.** After processing the blood, cells were fixed with 4% paraformaldehyde, and subsequently permeabilized with 0.2% Triton X-100 (Sigma-Aldrich) in PBS. Cells were immunostained with primary antibodies, biotin-Mouse monoclonal Cytokeratin 18 (Lifespan), and mouse monoclonal CD45-APC (ThermoFisher), followed by Yellow-Avidin nanobeads (Invitrogen) (1:2,500) to visualize the CTCs. All of the antibodies were prepared in 100 μl PBS plus 1% BSA and 0.1% Tween20 and chips were stained for 60 min at a flow rate of 100 μl $h^{-1}$. Chips were washed using 200 μl 0.1% Triton X-100 in PBS, at 0.6 ml $h^{-1}$ for 10 min. Chips were stained with the Yellow-Avidin nanobeads for 30 min at a flow rate of 200 μl $h^{-1}$, and subsequently washed with 200 μl of 0.1% Triton X-100 in PBS, at 600 μl $h^{-1}$ for 10 min. Nuclei were stained with 100 μl DAPI ProLong Gold reagent (Invitrogen) at 600 μl $h^{-1}$. After completion of staining, all devices were washed with PBS and stored at 4 °C before scanning.

**Antibodies.** The following antibodies were used in this study: CD326 (EpCAM) microBeads (130-061-101, MACS-dextran ferrite colloids beads with a diameter of 50 nm, purchased from Miltenyi Biotec), pan-Cytokeratin antibody [C-11]-APC (GTX80205); CD45 mouse anti-human mAb (clone HI30)-Alexa Fluor 488 (MHCD4520); anti-human CD326 (EpCAM)-Alexa fluor 647 (324212); anti-mouse H-2Kd- Alexa fluor 488 (116609); CK-18 mouse anti-human antibody clone C-04, biotin (LS-B9908), CD45-APC mouse anti-human clone HI30 (MHCD4505), yellow- Avidin nanobeads (F8771), DAPI nuclear stain (R37605), FcR blocking reagent (130-059-901).